J. Am. Ceram. Soc., 1–8 (2015)
DOI: 10.1111/jace.13919

journal

A Method for Determining Bulk Density, Material Density, and Porosity of Melter Feed During Nuclear Waste Vitrification

Zachary Hilliard† and Pavel Hrma

Pacific Northwest National Laboratory, Richland, Washington

Glassmelting efficiency largely depends on heat transfer to reacting glass batch (melter feed), which in turn is influenced by the bulk density (ρ_b) and porosity (ϕ) of the reacting feed as functions of temperature (T). Neither $\rho_b(T)$ nor $\phi(T)$ functions are readily accessible from direct measurements. For the determination of ρ_b, we monitored the profile area of heated feed pellets and calculated the pellet volume using numerical integration. For the determination of ϕ, we measured the material density of feeds quenched at various stages of conversion via pycnometry and then computed the feed density at heat-treatment temperature using thermal expansion values of basic feed constituents.

I. Introduction

The enormous task of turning more than 200 000 m^3 of Hanford nuclear waste into glass poses two major challenges: minimizing the product volume and maximizing the rate of production.[1] The first task, product minimization, was successfully solved using mathematical modeling based on glass property–composition functions.[2] The second challenge, accelerating the production rate, requires detailed understanding of the feed-to-glass conversion process as a function of melter-feed makeup,[3,4] i.e., the selection of mineral forms of the glass-forming and glass-modifying minerals and chemicals that are mixed with the waste to produce durable glass. The subject of this article is related to the second challenge.

The melter feed responds to heating with complex interactions. In the waste glass melter, this conversion process is confined to a relatively small region of space called the cold cap, a layer of reacting feed that covers the surface of molten glass.[5] Figure 1 schematically illustrates the cold cap profile. The top part of the cold cap allows reaction gases to escape through open pores to the atmosphere. In the bottom part, the glass-forming melt is connected, trapping evolving gases that turn it into primary foam. Simultaneously, gas bubbles (mainly oxygen from redox reactions and from the release of dissolved gases) ascend from the melt below the cold cap and create secondary foam. If the feed is charged into the melter in the form of slurry, part of the cold cap is covered with boiling suspension. In this case, the temperature within the cold cap spans as much as 1000 K. Most of the heat for the feed-to-glass conversion comes from the pool of hot melt below the cold cap. The foam layers, by limiting this heat flow, impede the rate of melting.

Attempts to mathematically represent the melting process in glass tanks were reviewed by Kuhn.[6] Pokorny and Hrma[7,8] developed a mathematical model of the cold cap, such as that illustrated in Fig. 1, which allows relating the glass production rate to the melter-feed properties as functions of the degree of conversion as is evolves in response to increasing temperature. These properties, such as heat conductivity and bulk density, are parameters in the field equations that, together with the boundary conditions, describe heat transfer, chemical reactions, phase transitions, and other processes that occur within the cold cap. These properties are functions of feed composition (in terms of both phases and chemistry) and porosity (i.e., the gas-phase volume fraction). As Fig. 1 indicates, the porosity reaches the highest values near the cold cap interface with molten glass. This article presents a methodology for determining the bulk density and porosity as functions of temperature for a melter feed heated at a constant rate.

II. Volume Expansion Test

Historically, various methods have been used to assess the rate of melting. The batch-free time method is perhaps most common for commercial applications.[9] A more quantitative approach was developed by Raether and Krauss who monitored the change in volume of a batch cone during heating.[10] Two additional methods have recently been employed for ranking feeds for nuclear waste glasses, namely, the vertical gradient furnace (VGF) test[11] and x-ray computed tomography (CT).[12] The VGF method mimics, in a crucible sample, the temperature gradient that exists between the plenum and the glass pool in a waste glass melter. The x-ray CT method subjects a quenched sample to a known x-ray spectrum and determines, by measuring the attenuation of the x-rays through the sample, how much unreacted feed and melt are present.

A method of visually observing and photographically recording the behavior of glass batch placed in a transparent silica glass crucible was first applied by Nemec to study the mechanism of bubble removal from molten glass.[13] This method has since been applied to monitoring the volume changes of dry melter feeds during heating.[14,15] The main disadvantage to this method is that the walls of the crucible can cause an undesirable bridging effect.

The volume expansion test is similar to Raether and Krauss' method except that the initial sample is a cylindrical pellet.[15,16] Both methods avoid wall effects that cause bridging of the foam and thus prevent obtaining the correct feed volume data. The main advantage of recording feed volume is a possibility to evaluate bulk density and porosity from the data and represent them as functions of temperature and heating rate for use in mathematical models. A feed pellet of known composition, mass, and dimensions (approximately 13 mm in diameter and 6 mm in height but varies slightly with each pellet and is measured to ±0.01 mm) is heated inside a furnace while pictures are taken of the pellet profile at various temperatures (see Fig. 2). The temperature ranges from room temperature to 1100°C and over 40 pictures are taken at decreasing temperature intervals. From room temperature to 600°C, there is one picture taken every 100°C.

E. Vance—contributing editor

Manuscript No. 36784. Received April 24, 2015; approved August 3, 2015.
†Author to whom correspondence should be addressed. e-mail: zachary.hilliard@pnnl.gov

The interval changes to approximately 25°C until 800°C at which point a picture is taken every 10°C until 1100°C. It is critical to keep the camera in the same position and resolution setting for the duration of the test so that the scale of the images remains constant. The following section describes the computation of the pellet volume from its profile by means of numerical integration.

Nomenclature	
A	Area
a	Diameter of top surface of volume element
b	Diameter of bottom surface of volume element
c	Phase mass fraction
g	Melt component mass fraction
h	Height of volume element
m	Mass
p	Material property
T	Heat treatment temperature
V	Volume
Greek letters	
α	Volumetric thermal expansion coefficient
β	Heating rate
δ	Picture scale (mm per pixel)
θ	Angle of slant
λ	Normalized quartz fraction
ρ	Density
ϕ	Porosity
Subscripts	
a	Actual
b	Bulk
g	Glass transition
M	Melt
p	Primary foam temperature
px	Pixel
Q	Quartz
s	Silica
Superscripts	
G	Final glass
s	Solid phase
m	Molten phase
Markers	
$\hat{\rho}$	quenched sample property p

III. Pellet Volume

When heated, the pellet shape changes during the heat treatment from the circular cylinder until it finally becomes a sessile drop (a melt droplet on a solid substrate). Assuming that the pellet remains throughout the heating process a quasi body of revolution (a body of circular cross sections that does not necessarily have an axis of revolution), its volume is generated by taking the width of the profile to be the diameter of a disk, the circumference of which is coincident with the profile and its height is differential. The relative error in bulk density produced by the difference, ΔV, between the calculated volume and actual volume is effectively offset at high temperatures at which the pellet volume oscillates by the formation and collapse of bubbles. It is reasonable to assume that the calculated volume is somewhere in the range of those oscillations. Before the formation of bubbles, the pellet is symmetrical so that ΔV is small.

Previously, the volume calculations were done by sectioning the pellet profile into thin horizontal segments and summing the volumes of the corresponding cylindrical disks (see Fig. 3). A platinum wire was used as a scale gauge.[16] This procedure has been improved using a computer program capable of increasing the number of elements and computing the volume efficiently and more accurately.

MATLAB's photo processing toolbox allows us to determine the pellet boundary with a one-pixel vertical spacing to achieve the best possible numerical volume approximation (Fig. 4). The boundary is split into the left (shown in white) and the right (shown in black) "sub-boundaries," each containing the same number of points that span the same vertical displacement. The algorithm that determines which pixels are located at the boundary searches row by row from left to right to find the left sub-boundary and right to left to find the right sub-boundary. The first pixel in a given row that satisfies certain conditions is then chosen to be a boundary pixel.

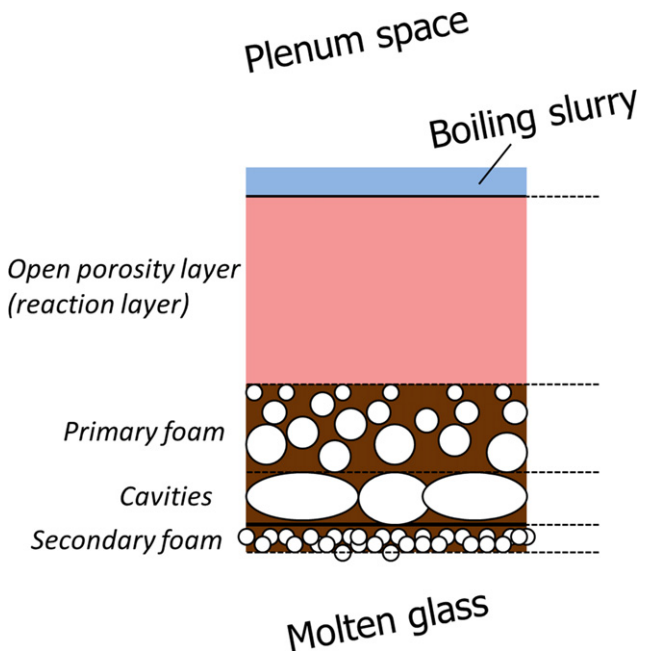

Fig. 1. Illustrative diagram of the cold cap.[8]

Points are defined at each boundary pixel so that trapezoidal profile elements are formed. This is possible because both the left and right boundaries have the same number of pixels. Volume elements are then constructed by letting each trapezoid be the profile of a slanted conical frustum volume element shown in Fig. 5, where the cone proportions are deliberately exaggerated. The actual cone is a thin disk with $h \ll a \approx b$.

The volume of the ith volume element, V_i, and the area, A_i, of the corresponding area element are expressed as:

$$V_i = \frac{\pi}{12}(a_i^2 + a_i b_i + b_i^2)h_i \tag{1}$$

and

$$A_i = \frac{(a_i + b_i)h_i}{2} \tag{2}$$

where a_i is the ith trapezoid top edge length, b_i is the ith trapezoid bottom edge length, h_i is the ith trapezoid height (equal to the distance between two adjacent pixels), and i ranges from 1 to N, where N is the number of pixels that the pellet spans in the vertical direction. Note that the degree to which the cone is slanted (θ in Fig. 5) has no effect on either the volume or the area.

The initial pellet at room temperature is in the form of a cylinder with known height and diameter. This allows us to define a scaling factor as:

$$\delta = 0.5\left(\sqrt[3]{V_a/V_{px}} + \sqrt{A_a/A_{px}}\right) \tag{3}$$

where $V_{px} = \Sigma_N V_i$ and $A_{px} = \Sigma_N A_i$; the subscripts a and px refer to the pellet and the cubic (or square) pixel, respec-

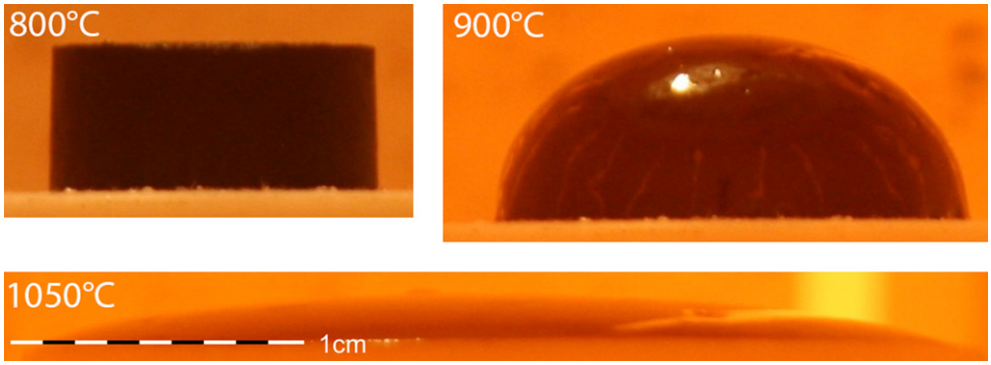

Fig. 2. Sample pictures from a volume expansion test. The images are identically scaled.

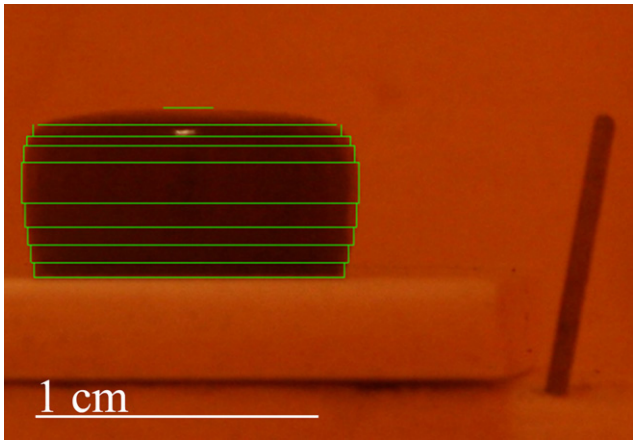

Fig. 3. Volume computation method based on cylindrical segments.

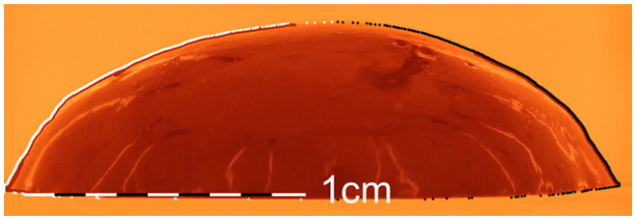

Fig. 4. Boundary pixels; the picture was manually edited to make the boundary more distinct.

tively. A proof for this equation is given the Appendix. The physical representation of δ is the magnitude of the displacement in the pellet plane (the plane in which the outermost edge of the pellet profile lies) which is the result of moving from the center of one pixel to the center of an adjacent pixel. Thus, the pellet volume becomes $V = \delta^3 \Sigma_N V_i$.

Obtaining the pellet volume as a function of temperature and heating rate is an exercise in geometry. Determining the bulk density and porosity necessitates additional information about the conversion process. The next section briefly describes its main features.

IV. Feed-to-Glass Conversion Process

The melter feed to be processed in the vitrification plant is a mixture of tank waste with glass-forming and glass-modifying additives. The Hanford tank waste has aged for more than 50 yr in underground tanks, mostly in the form of sludge submerged under supernatant. In the laboratory, we prepare nonradioactive melter-feed simulant by making a slurry to which chemicals are added in a prescribed order.[17] The slurry is dried before thermal processing in crucibles.

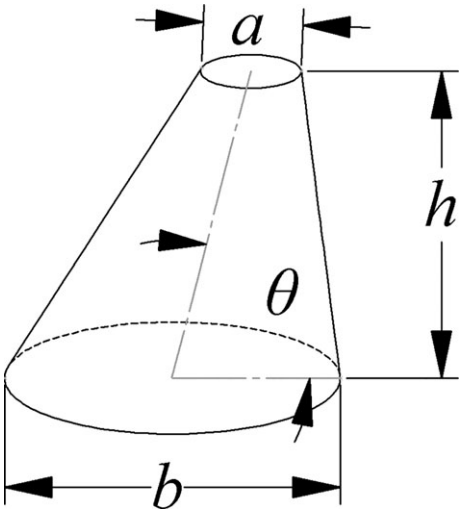

Fig. 5. Volume element.

Some chemicals react in the aqueous environment and during drying (e.g., sodium hydroxide reacts with boric acid creating sodium borates).[15,18] In the melter, slurry feed dries at a rate depending on the heat transfer from both the cold cap and the plenum space. Thus, the industrial process and its laboratory simulation are not exactly equal. We consider these differences in feed preparation and processing as minor, not significantly affecting the applicability of model based on laboratory data to the feed-to-glass conversion that occurs in the actual cold cap. Only when the simulated feed is sufficiently developed, the real tank waste is used for the final checkup.

As the dry feed is heated, whether in a crucible or in a large-scale melter, it undergoes multiple chemical reactions, mostly releasing bonded H_2O, CO, CO_2, N_2O, NO, and O_2. Inorganic salts melt, forming low-temperature eutectics. While reacting with other feed components, they produce intermediate crystalline phases. Glass-forming melt is a product of reactions of feed components, such as amorphous hydroxides and oxyhydrates, first with borates, and then with quartz and silicates. Intermediate crystalline phases, such as hematite, various spinels, nepheline, or crystals with sodalite structure, are common.[19]

The feed-to-glass conversion is a kinetic process of colossal complexity. The material parameters associated with this process, such as bulk density and heat conductivity, are changing in response to the changes of fractions, configuration, and chemical composition of the phases present. These parameters cannot be measured directly which makes the use of various analytical tools necessary.

The bulk density is defined as $\rho_b(T) = m(T)/V(T)$. The pellet mass, m, is obtained as $m(T) = m_0[1-f(T)]$, where m_0 is the initial mass and $f(T)$ is the mass loss fraction. The mass

loss fraction has been determined by thermogravimetric analysis (TGA), see Fig. 6.

Determining the porosity is more challenging. The porosity, ϕ, is the ratio of the gas-phase volume, V_v, to the pellet volume, V, i.e., $\phi = V_v/V$. This expression can be written in terms of the bulk density, ρ_b, and the material density (i.e., the density of the condensed phase; the gas phase is not included), ρ:

$$\phi(T) = 1 - \frac{\rho_b(T)}{\rho(T)} \tag{4}$$

The next section describes how the high-temperature material density, ρ, is estimated based on the measured density of rapidly quenched heat-treated feed samples, the composition and thermal expansion of the condensed phases, and the glass transition temperature of the glass-forming phase.

V. Material Density

The conversion of melter feed to molten glass results in changes in the material density (i.e., the density of the condensed phase, which is a mixture of all solids and liquids in the reacting feed). Initially, the condensed phase density increases as the molten salts and hydroxides gradually turn into crystalline oxides. This trend is reversed once enough glass-forming phase accumulates and the material density begins to decrease as the crystalline phases dissolve, becoming amorphous.

The material density of a mixture of phases is given by the formula $\rho = (\Sigma_N c_i/\rho_i)^{-1}$, where c_i is the ith phase mass fraction and ρ_i is the ith phase density. The individual phases can be liquid and solid, amorphous and crystalline. Estimating their content and high-temperature densities based on thermal expansions and phase transition temperatures would be a tedious task burdened with large uncertainty that would exceed uncertainties associated with errors in the pellet volume caused by the deviations of the shape of a melted pellet from a quasi body of revolution and possible deviations of the camera angle from the horizontal plane.

This situation simplifies when the number of phases decreases to a few in the temperature at which the glass-forming phase becomes continuous, which is the interval of interest for a good assessment of the sample porosity by Eq. (4). At this advanced stage of conversion, at least for high-level waste feeds, almost all chemical reactions and phase transitions are complete except for the dissolution of quartz particles. The content of other solid phases, mainly spinel, is small and can be neglected. In the following paragraphs, we assume that this is the case. If slow-dissolving silicate minerals from the feed continue to dissolve in the foaming temperature interval, as may be the case of low-activity waste glasses,[20] the analysis can easily be extended to include them.

The temperature at which the glass-forming phase is fully connected (T_p) is marked by a minimum on the volume–temperature curve from the volume expansion test (this temperature is identical with the primary foam temperature denoted as T_P in the cold cap modeling papers[8]). Considering that only two condensed phases, melt and quartz, make the sample at $T \geq T_p$, the reacting feed material density can be expressed as:

$$\rho(T) = \frac{1}{\frac{1-c_Q(T)}{\rho_M(T)} + \frac{c_Q(T)}{\rho_Q(T)}} \tag{5}$$

where M stands for melt and Q for quartz.

At the glass transition temperature, T_g, the volume expansion coefficient of the glass-forming phase abruptly changes while the density remains a continuous function of temperature. The T_g and the expansion coefficients of the molten glass (the glass-forming phase) below and above the T_g change as the melt composition changes in response to the dissolving quartz. The silica fraction in melt increases from nearly zero at T_p to the final fraction of the homogeneous glass with quartz completely dissolved. Here we use the average composition of the melts, ignoring concentration gradients associated with the diffusion-driven dissolution and homogenization.

Using for a glass property–composition relationship the linear function:

$$p = \Sigma_N p_i g_i \tag{6}$$

where p is a property, g_i is the ith component mass fraction, and p_i is the ith component partial specific property, and recollecting that $\Sigma_N g_i = 1$, the response of p to the change in added silica can be expressed as:

$$p(T) = p_s g_s(T) + [p^G - p_s g_s^G(T)]\frac{1 - g_s(T)}{1 - g_s^G} \tag{7}$$

where the superscript G denotes the final glass and s denotes silica. Using the relationship $c_Q(T) = \frac{g_s^G - g_s(T)}{1 - g_s(T)}$ (easily seen by examining the difference $g_s^G - g_s(T)$ using mass conservation),

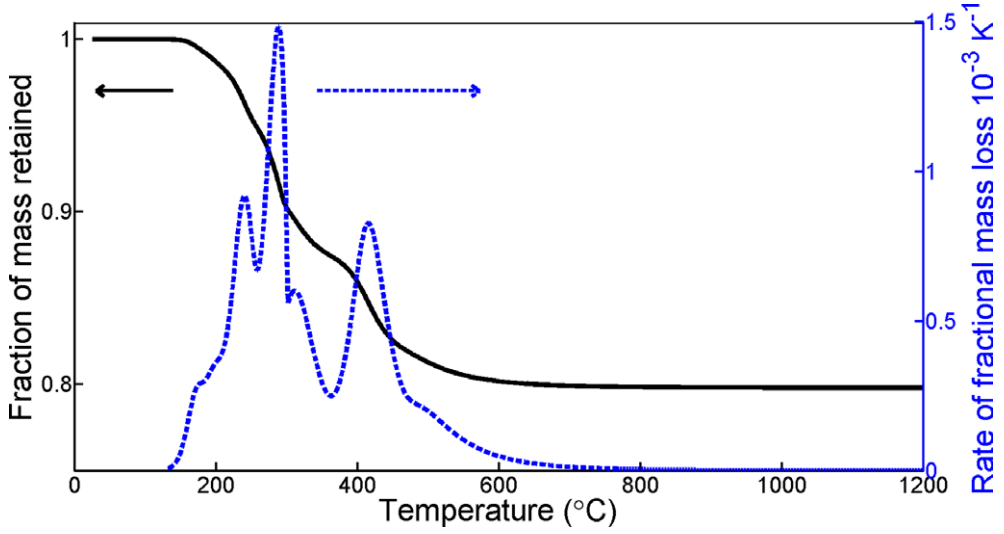

Fig. 6. Mass loss and mass loss rate from a HLW feed heated at 10 K/min.[16,21]

Eq. (7) can be rewritten as:

$$p(T) = \frac{p^{G} - p^{s} c_{Q}(T)}{1 - c_{Q}(T)} \tag{8}$$

The thermal volumetric expansion coefficient is defined as $\alpha \equiv \frac{1}{V}\frac{dV}{dT}$. For $T < T_g$, $\alpha = \alpha_S$, where α_S is the solid glass thermal expansion; for $T > T_g$, $\alpha = \alpha_L$, where α_L is the molten glass thermal expansion. Using these values, the melt density can be approximated as:

$$\ln\left(\frac{\rho_M(T)}{\hat{\rho}_M(T)}\right) = a_s(T)(T_0 - T) + [a_s(T) - a_L(T)] \\ [T - T_g(T)]\mathcal{H}(T - T_g(T)] \tag{9}$$

where the functions $\alpha_S(T)$, $\alpha_L(T)$, and $T_g(T)$ have the form of Eq. (8) and $\hat{\rho}_M(T)$, the room-temperature material density of the melt condensed phase, can be found by applying Eq. (5) to the known function $\rho_0(T)$; $\mathcal{H}$ is the Heaviside step function. In this simplified model, we ignore the change in the crystal structure of quartz and assume that only volume expansion affects quartz density between T_0 and T.

Table I summarizes data for a melter feed, labeled A0, which was developed to vitrified high-level high-alumina simulated nuclear waste. This particular feed was well characterized in previous cold cap studies.[7,8,15–18,21–28]

Based on the kinetic model for the quartz fraction in A0 feed,[18] c_Q can be calculated as a function of both heating rate and temperature using the equation:

$$c_Q(T, \beta) = g_s^G \lambda(T, \beta) \tag{10}$$

where $\lambda(T, \beta)$ is the normalized quartz fraction from the kinetic model and β is the heating rate in K/min. The shape of $\lambda(T, \beta)$ is such that $\lambda(T, \beta)$ is close to 1 at $T < T_p$ when no quartz is dissolved and close to 0 when all quartz is dissolved. The material density of quenched A0 feed, which was measured by pycnometry on powdered room-temperature samples heat treated at 5 K/min,[27] was fitted with the function:

$$\rho_0(T) = a_1 + a_2 \tan^{-1}\left(\frac{T - T_1}{T_2}\right) \\ + a_3(T - T_5)^2 \exp\left(-\left(\frac{T - T_3}{T_4}\right)^2\right) \tag{11}$$

where the coefficients are listed in Table I.

The $\rho(T)$ function was evaluated using Eq. (8) to obtain α_S, α_L, and T_g as functions of the composition of the quartz-melt mixture, which changed with the heat-treatment temperature according to Eq. (10). With coefficient values summarized in Table I, calculation was performed for the temperature interval from $T_p = 820$°C (determined by the temperature at which the minimum volume occurred) to 1200°C. For the temperature interval from $T_0 = 100$°C to T_p, the density was estimated using the linear interpolation $\rho(T) = \hat{\rho}(T) + (T - T_0)\frac{\rho(T_p) - \hat{\rho}(T_p)}{T_p - T_0}$. The resulting $\rho = \rho(T)$ function is plotted in Fig. 7 alongside $\rho_0 - \hat{\rho}(T)$ for comparison.

Table I. Coefficients and Data

Coefficients for Eq. (11)[27]			Data from Literature			References
a_1	g/cm	2.492	g_S^G	—	0.305	[17]
a_2	g/cm	0.0106	α_S^G	K^{-1}	3.76E-5	[28]
a_3	g/cm	5.65E-6	α_L^G	K^{-1}	2.40E-4	[28]
T_1	°C	534	α_S^s	K^{-1}	4.90E-6	[28]
T_2	°C	123	α_L^s	K^{-1}	1.71E-4	[28]
T_3	°C	184	T_g^G	°C	469	[34]
T_4	°C	389	α_g^s	°C	634	[34]
T_5	°C	100	α_Q	K^{-1}	1.75E-5	[35]
			$\hat{\rho}_Q$	g/cm	2.648	[36]

VI. Porosity

Figure 8 shows the normalized volume and fractions of both the condensed phase and the gas phase (the porosity) plotted versus temperature. The porosity values were calculated using data given in Section 5 and the kinetic mass loss model developed for A0 feed[21] (Fig. 6). The porosity evolves in four distinct stages:

1. From 25°C to 600°C, the pellet volume slightly decreases while the density increases and the mass decreases by approximately 20%. The density increase in combination with the mass decrease results in a significant decrease in material volume fraction so that the porosity (open at this stage) increases to a maximum in the neighborhood of 600°C.
2. From 600°C to 800°C, the porosity (which remains mostly open) decreases and the condensed phase volume fraction increases following the decrease in pellet volume.
3. From 800°C to 925°C, the pellet volume rapidly increases because of a similarly rapid increase in porosity caused by the continuous evolution and thermal expansion of gases in the connected melt. The continuing decrease in material density has a negligible effect.
4. Finally, above 925°C, the collapsing of foam bubbles into the atmosphere causes a general decrease in the both the pellet volume and the porosity. The decrease is not monotonic, but somewhat oscillatory because of the simultaneous growth and collapse of bubbles.

The cumbersome calculations involved in computing the high-temperature material density (Section V) may be avoided if $\rho(T)$ is approximated as $\rho_0(T)$. As Fig. 9 indicates, this approximation yields a reasonable ϕ(T) function, at least for A0 feed, and is useful for model applications where the errors produced are tolerable or the values of the coefficients listed in Table I are lacking or difficult to obtain.

VII. Discussion

To represent a material particle of feed as it is gradually converted to glassmelt within the cold cap, the pellet must be sufficiently homogeneous in temperature and composition. The temperature history of the pellet can be adjusted as close as needed to that a feed particle experiences in the cold cap. The initial feed density difference caused by pellet compaction has little effect on the conversion process, especially at higher temperatures where the solid feed becomes a liquid droplet. Unlike the pellet, the feed particle in the cold cap is exposed to its own atmosphere, but the vigorous gas evolving reactions are hardly affected by this difference at the open-porosity stage. Then, at the foaming stage, when the pellet turns into a droplet, we can assume that bubbles grow and coalesce in the same way as in the cold cap. When large bubbles finally open to the atmosphere from the droplet, the mechanism is most likely similar to that of bubbles merging into gas cavities below the cold cap.

Since foam controls the heat flux from the melt pool to the reacting zone, the foaming stage is crucial for the rate of melting. Therefore, the main concern is whether the mode of foam development and collapse in the sessile droplet is similar to that in the cold cap. As argued above, one can assume that the difference is little at least for melters in which the melt convection is natural, driven by buoyancy.

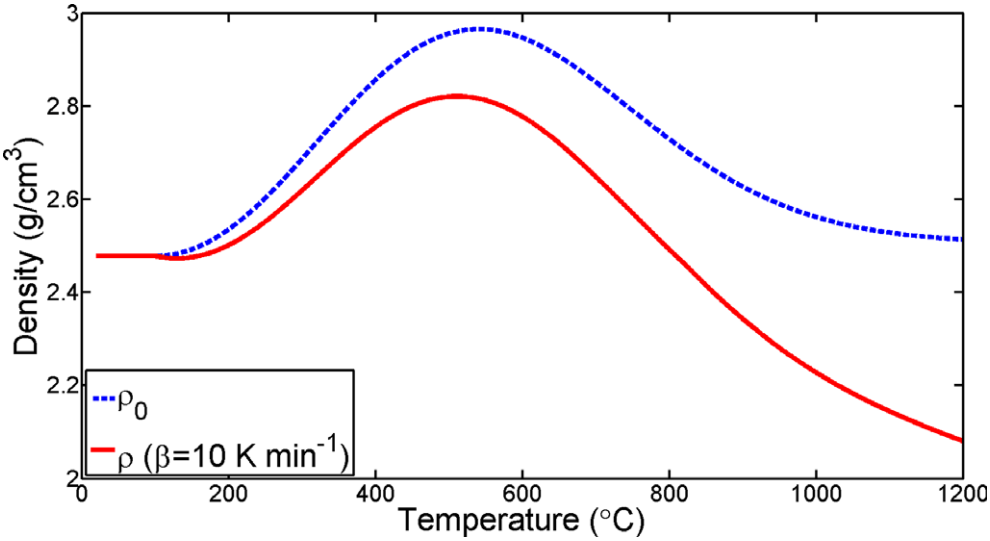

Fig. 7. Condensed phase density for A0 heated at 10 K/min.

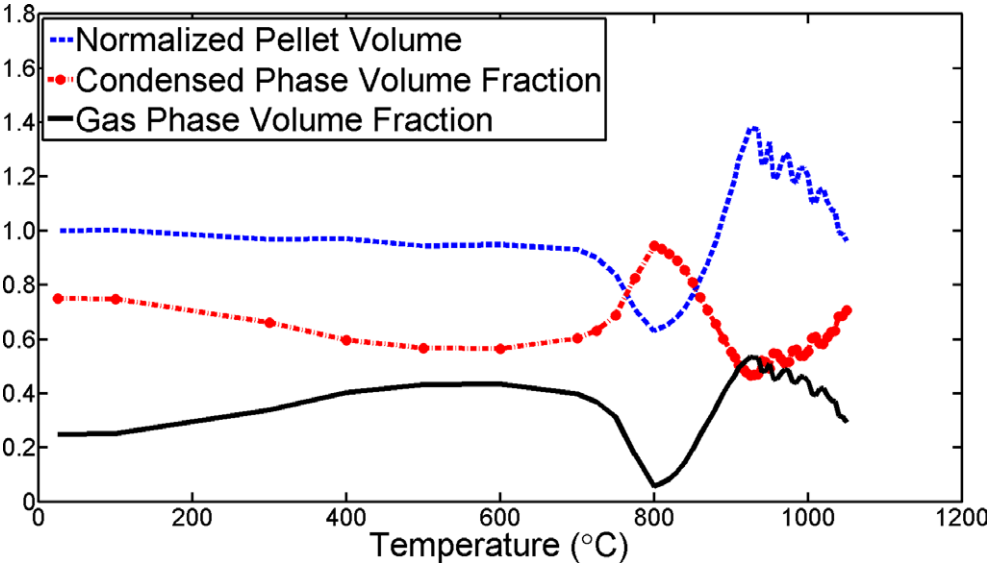

Fig. 8. Normalized pellet volume and phase volume fractions for A0 feed at 10 K/min.

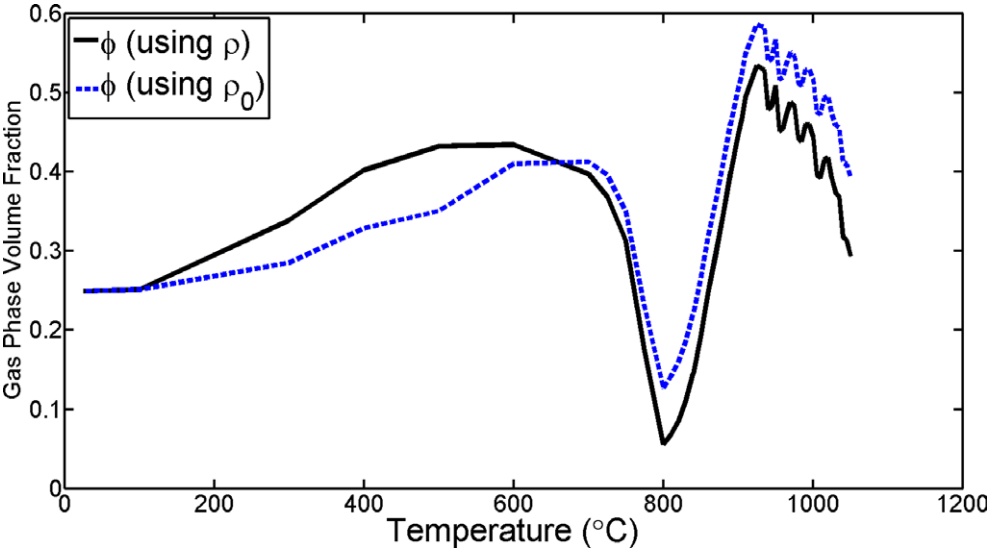

Fig. 9. Gas-phase volume fraction calculated with $\rho = \rho(T)$ compared with the gas-phase volume fraction calculated with $\rho = \rho_0(T)$.

However, melters processing nuclear waste glasses are often equipped with bubblers installed under the cold cap. In such melters, powerful forced convection is driven in molten glass by ascending large bubbles that bring hot melt into direct contact with the cold cap bottom, sweeping away secondary foam (accumulation of tiny bubbles rising from the melt pool, see Fig. 1) and gas cavities.[29] Depending on the foam extent and melt viscosity, an exceptionally strong forced convection may carry away even a part of primary foam. If this is the case, the correspondence between the pellet response and cold cap behavior will have to be carefully evaluated.

The objective of cold cap studies is to help optimize the glassmelting process through an advanced formulation of melter feeds. The simple inexpensive volume expulsion test is a handy technique that can minimize the effort needed for execution of melter experiments. Experiments performed with pellets from feeds other than A0, a high-alumina feed chosen for this work because of the availability of data needed for density and porosity evaluation, show that volume changes in response to heating can widely differ depending on the gas evolution rate and melt formation rate as functions of temperature.[30–33] This diversity of responses may challenge the formulation of $\rho_b(T)$ and $\phi(T)$ approximation functions that are essential for cold cap modeling. These functions will also be useful for quantifying the effects of feed makeup variations, such as quartz particle size or the chemical and mineralogical form of the feed additives, on the feed foaming extent and, hence, on the impact of feed formulation on cold cap behavior, including the rate of melting.

VIII. Conclusion

Mathematical modeling of glassmelting, or feed-to-melt conversion, as it occurs in the cold cap requires the knowledge of the bulk density as a function of the degree of conversion, or equivalently, as a function of the temperature and rate of heating. Additionally, knowledge of the porosity function is necessary to calculate the heat conductivity and determine the completion of the feed-to-glass conversion.

Bulk density data can be obtained using a volume expansion measurement of the feed via the volume expansion test in conjunction with TGA. Assuming that the pellets retain the geometry of a quasi body of revolution during the conversion process, a simple algorithm then converts the pellet profile to pellet volume using pixel counting and a scaling factor.

For the porosity calculation, additional information is needed, namely, the material (condensed phase) density as a function of temperature (i.e., the degree of conversion). The material density is estimated based on the density data of samples quenched from various temperatures along with data regarding the thermal expansions of the continuously interacting feed phases and the glass transition temperature of the glass-forming phase, whose composition changes as the conversion progresses. The program created allows the effect of the temperature and the heating rate on the porosity to be determined.

The improved pellet volume calculation method described in this article will allow for a more accurate determination of the bulk density and porosity functions that will be used in mathematical modeling of the heat transfer through the cold cap, and thus will help increase the rate at which the nuclear waste is vitrified.

Acknowledgments

Pacific Northwest National Laboratory is operated for the U.S. Department of Energy by Battelle under Contract DE-AC05-76RL01830. This work was supported by the U.S. Department of Energy's Waste Treatment and Immobilization Plant Federal Project Office under the direction of Dr. Albert A. Kruger. The authors thank David Pierce and Brad Vanderveer for data collection and Carmen Rodriguez for density measurement.

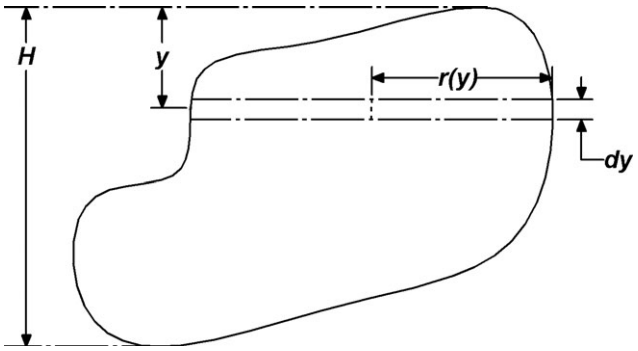

Fig. 10. Quasi body of revolution.

Appendix
Proof of Equation (3)

Let a three-dimensional body be considered where each transverse cross section is circular, but the body is not necessarily a body of revolution because there may not be an axis of revolution. See Fig. 10 below.

The volume and profile area of the body is given by Eqs. (12) and (13), where H is the height of the body and $r(y)$ is the radius of the transverse cross section at the height y:

$$V_1 = \pi \int_0^H r^2(y)\mathrm{d}y \tag{12}$$

$$A_1 = 2\int_0^H r(y)\mathrm{d}y \tag{13}$$

If the body dimensions are multiplied by some scalar δ (i.e., the scaling factor) so that the body is proportionally the same as stated earlier, the new volume and profile area are given by Eqs. (14) and (15):

$$V_2 = \pi \int_0^{\delta H} \delta^2 r^2\left(\frac{y}{\delta}\right)\mathrm{d}y \tag{14}$$

$$A_2 = 2\int_0^{\delta H} \delta r\left(\frac{y}{\delta}\right)\mathrm{d}y \tag{15}$$

After substituting $u = y/\delta$ into both equations and comparing the results to Eqs. (12) and (13), Eqs. (16) and (17) arise:

$$V_2 = \delta^3 V_1 \tag{16}$$

$$A_2 = \delta^2 A_1 \tag{17}$$

which can be rearranged so that $\delta = \sqrt[3]{V_2/V_1}$ and $= \sqrt{A_2/A_1}$. In the application used in this article, there is no guarantee that the pellet will be exactly a quasi body of revolution, so an average scaling factor is defined using the δ values defined in both Eqs. (16) and (17) is given as Eq. (18):

$$\delta = 0.5\left(\sqrt[3]{V_2/V_1} + \sqrt{A_2/A_1}\right) \tag{18}$$

If the volume of the pellet in cubic pixels (also sometimes referred to as voxels) is considered to be V_1 and the profile area of the pellet in square pixels is considered to be A_1, then

if the pellet is a quasi body of revolution there is some linear scaling factor that will convert the pixel volume and area to a more standard unit such as mm^3 and mm^2. Taking V_2 and A_2 to be the volume and area of the pellet in mm^3 and mm^2 at room temperature (the only temperature where the dimensions of the pellet can physically be measured), then the scaling factor at room temperature can be determined. In this case, the units would be in mm/pixel. As explained in the body of this article, the physical representation of δ is the magnitude of the displacement in the pellet plane (the plane in which the outermost edge of the pellet profile lies) which is the result of moving from the center of one pixel to the center of an adjacent pixel. This means that if neither the camera nor the pellet plane move, the scaling factor will remain constant throughout the experiment.

References

[1]R. A. Kirkbride, et al., "Tank Waste Remediation System Operation and Utilization Plan"; Vol. I, HNF-SD-WM-SP-012. Numatec Hanford Corporation, Richland, Washington, 1999.

[2]J. D. Vienna, D. C. Skorski, D. S. Kim, and J. Matyas, "Glass Property Models and Constraints for Estimating the Glass to be Produced at Hanford by Implementing Current Advanced Glass Formulation Efforts"; PNNL-22631, Rev. 1. Pacific Northwest National Laboratory, Richland, Washington, 2013.

[3]M. Cable, "Principles of Glass Melting"; pp. 1–44 in *Classical Glass Technology*, Edited by D. R. Uhlman and N. J. Kreidl. Academic Press, Orlando, 1984.

[4]W. Trier, *Glass Furnaces: Design, Construction and Operation.* Society of Glass Technology, Sheffield, 1987.

[5]D. R. Dixon, M. J. Schweiger, and P. Hrma, "Effect of Feeding Rate on the Cold Cap Configuration in a Laboratory-Scale Melter"; WM2013 Conference, Paper 13362, Phoenix, Arizona, 2013.

[6]W. S. Kuhn, "Mathematical Modeling of Batch Melting in Glass Tanks"; pp. 73–125 in *Mathematical Simulation in Glass Technology*, Edited by D. Krause and H. Loch. Springer, Berlin, 2002.

[7]R. Pokorny and P. Hrma, "Mathematical Modeling of Cold Cap," *J. Nucl. Mater.*, **429**, 245–56 (2012).

[8]R. Pokorny and P. Hrma, "Model for the Conversion of Nuclear Waste Melter Feed to Glass," *J. Nucl. Mater.*, **445**, 190–9 (2014).

[9]M. Cable and M. Q. Siddiqui, "The Replacement of Soda Ash by Caustic Soda in Laboratory Glass Melting Trials," *Glass Technol.*, **21** [4] 193–8 (1980).

[10]F. Raether and M. Krauss, "*In Situ* Measurements of Batch Glass During Melting," *Glass Sci. Technol.*, **77** [3] 118–23 (2004).

[11]K. S. Matlack, I. S. Muller, H. Gan, I. Joseph, and I. L. Pegg, "Melter Tests to Define LAW Halide Concentrations, Phase 2, Test Plan"; VSL-13T3280-1, Rev. A. Vitreous State Laboratory, EnergySolutions Inc., Washington D.C., 2013.

[12]K. Watanabe, T. Yano, K. Takeshita, K. Minami, and E. Ochi, "X-ray CT Imaging of Vitrified Glasses Containing Simulant Radioactive Wastes: Structure and Chemical Reactions of Glass Beads and Wastes in the Cold Cap," *Glass Technol.: Eur. J. Glass Sci. Technol. A*, **53** [6] 273–8 (2012).

[13]L. Nemec, "Refining of Glass Melts," *Glass Technol.*, **15** [6] 153–6 (1974).

[14]P. A. Smith, J. D. Vienna, and P. Hrma, "The Effect of Melting Reactions on Laboratory-Scale Waste Vitrification," *J. Mat. Res.*, **10** [8] 2137–49 (1995).

[15]P. Hrma, et al., "Effect of Glass-Batch Makeup on the Melting Process," *Ceram-Silikaty*, **54** [3] 193–211 (2010).

[16]S. H. Henager, P. Hrma, K. J. Swearingen, M. J. Schweiger, J. Marcial, and N. E. TeGrotenhuis, "Conversion of Batch to Molten Glass, I: Volume Expansion," *J. Non-Cryst. Solids*, **357**, 829–35 (2011).

[17]M. J. Schweiger, P. Hrma, C. J. Humrickhouse, J. Marcial, B. J. Riley, and N. E. TeGrotenhuis, "Cluster Formation of Silica Particles in Glass Batches During Melting," *J. Non-Cryst. Solids*, **356** [25–27] 1359–67 (2010).

[18]R. Pokorny, J. A. Rice, J. V. Crum, M. J. Schweiger, and P. Hrma, "Kinetic Model for Quartz and Spinel Dissolution During Melting of High-Level-Waste Glass Batch," *J. Nucl. Mater.*, **443** [1–3] 230–5 (2013).

[19]D. R. Dixon, M. J. Schweiger, B. J. Riley, R. Pokorny, and P. Hrma, "Temperature Distribution Within a Cold Cap During Nuclear Waste Vitrification,"*Environ. Sci. Technol.*, **49** [14] 8856–63 (2015).

[20]K. Xu, P. Hrma, J. Rice, M. J. Riley, M. J. Schweiger, and J. V. Crum, "Melter Feed Reactions at T = 700°C for Nuclear Waste Vitrification," *Am. Ceram. Soc.*, (2015). doi: 10.1111/JACE.13766.

[21]R. Pokorny, D. A. Pierce, and P. Hrma, "Melting of Glass Batch: Model for Multiple Overlapping Gas-Evolving Reactions," *Thermochim. Acta*, **541** [10] 8–14 (2012).

[22]J. A. Rice, R. Pokorny, M. J. Schweiger, and P. Hrma, "Determination of Heat Conductivity and Thermal Diffusivity of Waste Glass Melter Feed: Extension to High Temperatures," *J. Am. Ceram. Soc.*, **97** [6] 1952–8 (2014).

[23]R. Pokorny, A. A. Kruger, and P. Hrma, "Mathematical Modeling of Cold Cap: Effect of Bubbling on Melting Rate," *Ceram. Silikaty*, **58**, 296–302 (2014).

[24]C. Rodriguez, J. Chun, M. Schweiger, A. Kruger, and P. Hrma, "Application of Evolved Gas Analysis to Cold-Cap Reactions of Melter Feeds for Nuclear Waste Vitrification," *Thermochim. Acta*, **592**, 86–92 (2014).

[25]P. Hrma, K. J. Swearingen, S. H. Henager, M. J. Schweiger, J. Marcial, and N. E. TeGrotenhuis, "Conversion of Batch to Molten Glass, II: Dissolution of Quartz Particles," *J. Non-Cryst. Solids*, **357** [3] 820–8 (2011).

[26]P. Hrma and J. Marcial, "Dissolution Retardation of Solid Silica During Glass-Batch Melting," *J. Non-Cryst. Solids*, **357** [15] 2954–9 (2011).

[27]J. Marcial, J. Chun, P. Hrma, and M. Schweiger, "Effect of Bubbles and Silica Dissolution on Melter Feed Rheology During Conversion to Glass," *Environ. Sci. Technol.*, **48**, 12173–80 (2014).

[28]P. Hrma, et al., "Property/Composition Relationships for Hanford High-Level Waste Glasses Melting at 1150°C"; PNL-10359, Vol. 1 and 2. Pacific Northwest Laboratory, Richland, Washington, 1994.

[29]R. Pokorny, et al., "Cold Cap Model for Melters with Bubblers," *J. Am. Ceram. Soc.*, (2015). doi: 10.1111/jace.13775.

[30]P. Hrma, et al., "Increasing High-Level Waste Loading in Glass Without Changing the Baseline Melter Technology"; Waste Management'01. University of Arizona, Tucson, Arizona, 2001.

[31]J. G. Darab, E. M. Meiers, and P. A. Smith, "Behavior of Simulated Hanford Slurries During Conversion to Glass," *Mat. Res. Soc. Proc*, **556**, 215–22 (1999).

[32]T. Jin, D.-S. Kim, A. E. Tucker, M. J. Schweiger, and A. A. Kruger, "Reactions During Melting of low-Activity Waste Glasses and Their Effects on the Retention of Rhenium as a Surrogate for Technetium-99.," *J. Non-Cryst. Solids*, **425**, 28–45 (2015).

[33]K. Xu, D. A. Pierce, P. Hrma, M. J. Schweiger, and A. A. Kruger, "Rhenium Volatilization in Waste Glasses," *J. Nucl. Mater.*, **464**, 382–8 (2015).

[34]P. Hrma, "Glass Viscosity as a Function of Temperature and Composition: A Model Based on Adam-Gibbs Equation," *J. Non-Cryst. Solids*, **354** [29] 3389–99 (2008).

[35]Y. Linard, H. Nonnet, and T. Advocat, "Physicochemical Model for Predicting Molten Glass Density," *J. Non-Cryst. Solids*, **354** [45–46] 4917–26 (2008).

[36]"Physical Constants of Inorganic Compounds," in *CRC Handbook of Chemistry and Physics, Internet Version*, pp. 4–82, Edited by D. R. Lide. http://www.hbcpnetbase.com, accessed on 29/12/2014 CRC Press, Boca Raton, Florida, 2005. □